

## Structural and magnetic properties of Cu/Fe multilayers

D. W. Lee, D. H. Ryan, Z. Altounian, and A. Kuprin

*Centre for the Physics of Materials, Department of Physics, McGill University, Montreal, Quebec, Canada H3A 2T8*

(Received 19 February 1998; revised manuscript received 20 July 1998)

The structural and magnetic properties of Cu/Fe multilayers, prepared by dc-magnetron sputtering on silicon substrates, have been studied as a function of Fe layer thickness  $t_{\text{Fe}}$ , from 7 to 34 Å. Structural characterization confirmed the successful growth of high-quality layered structures along the film growth direction, and showed an increasing contribution from interface roughness with decreasing  $t_{\text{Fe}}$ . Magnetoresistance (MR) showed an evolution from well-defined superlattice to granular behavior with decreasing  $t_{\text{Fe}}$ . For  $t_{\text{Fe}} < 7$  Å the island structure was confirmed by observing superparamagnetic blocking in ac susceptibility. The temperature dependence of the magnetization suggests that for  $t_{\text{Fe}} = 7$  Å, 75% of the Fe atoms are in a superparamagnetic Fe phase, leaving the remaining 25% as a Cu-Fe alloy. A gradual evolution in magnetic behavior from ferromagnetism to paramagnetism with decreasing  $t_{\text{Fe}}$  was also seen using conversion-electron Mössbauer spectroscopy (CEMS). We observed a monotonic decrease in average hyperfine field of the magnetic components in the CEMS data, coupled with increasing areas of two interfacial phases. For  $t_{\text{Fe}} \leq 10$  Å a paramagnetic component develops which we identified as islands of fct-Fe. We attribute the change in magnetic behavior in this system with decreasing  $t_{\text{Fe}}$  to an evolution from multilayer to island structures rather than to the formation of a nonmagnetic fcc-Fe phase. [S0163-1829(99)03609-7]

### I. INTRODUCTION

Band-structure calculations have suggested that the magnetic properties of transition-metal ferromagnets are extremely sensitive to atomic density<sup>1-3</sup> and thin films are ideal structures in which to study such behavior. It is possible to vary both lattice spacing and crystal structure by growing a thin layer of a material on a stable buffer layer with a suitable lattice constant. The Cu/Fe system is particularly interesting<sup>4-13</sup> because fcc  $\gamma$ -Fe can be stabilized down to low temperatures either as small Fe precipitates in a Cu matrix or as thin epitaxial Fe films on a Cu buffer layer.<sup>8</sup> Epitaxial Cu/Fe multilayers are possible because of the similarity of lattice constants of Cu (3.615 Å at 295 K) and  $\gamma$ -Fe [3.588 Å at 293 K, extrapolated from bulk  $\gamma$ -Fe data above 1185 K,<sup>6</sup> or 3.5757 Å at 80 K measured for  $\gamma$ -Fe precipitates in Cu (Ref. 19)].

Since the report by Jesser and Matthews,<sup>4</sup> there has been a wealth of information in the literature on epitaxial growth of Fe by evaporation onto Cu.<sup>7-9,11-13</sup> Their results show that Fe undergoes complicated structural changes and that the magnetic behavior of Fe indeed correlates with its structural changes. Recently, several groups<sup>9,11,12</sup> have suggested that the room temperature (RT) growth of Fe on Cu(100) leads to three distinct phases: (1) a ferromagnetic fct (face-centered-tetragonal) structure for films less than 5 monolayers (ML); (2) an antiferromagnetic bulk fcc structure with a ferromagnetically ordered surface layer for films between  $\sim 5$  and 11 ML; and (3) a ferromagnetic bcc structure for films thicker than  $\sim 13$  ML.

While most of the work on fcc Fe has been done on bilayers with a simple Fe film grown by evaporation on a Cu substrate, very few studies on Cu/Fe multilayered thin films have been reported.<sup>5,10,14,15</sup> Recent work by Cheng *et al.*<sup>10</sup> on magnetron-sputtered Fe/Cu multilayers using extended x-ray-absorption fine-structure spectroscopy suggested that

the crystal structure of Fe changes from distorted bcc to fcc with decreasing Fe layer thickness  $t_{\text{Fe}}$ . They found a fcc Fe sample to be ferromagnetic with a reduced Curie temperature. On the other hand, a Mössbauer study of evaporated Fe/Cu multilayers by Pankhurst *et al.*<sup>15</sup> showed that samples with 5-Å-thick Fe layers have roughly equal quantities of ferromagnetic bcc Fe and antiferromagnetic fcc Fe. The additional complications introduced by the growth of multilayer samples can make the study of the structural dependence of the magnetic properties more difficult. For example, the two surfaces of the Fe layer (Cu/Fe and Fe/Cu) need not be identical. Furthermore, structural imperfections can lead to the formation of an island structure with dislocated submultilayers for ultrathin Fe layers. This may produce a composite granular solid which consists of nanometer-sized Fe grains embedded in the Cu medium and may exhibit superparamagnetic behavior.

In this study, we present a detailed study of structure, magnetotransport, and magnetic properties of magnetron-sputtered Cu/Fe multilayers. The iron thickness ( $t_{\text{Fe}}$ ) in Cu/Fe multilayers was varied systematically in order to change the atomic density of Fe. The aim of this study is to develop a fundamental understanding of the structural dependence of the magnetic properties. In particular, the possibility of superparamagnetic relaxation was studied carefully.

### II. EXPERIMENTAL METHODS

A series of Cu/Fe multilayers was prepared using dc magnetron sputtering onto silicon substrates with nominal individual layer thicknesses ranging from 25 down to 5 Å and total number of bilayers between 12 and 36. Base pressure before each deposition was less than  $2 \times 10^{-7}$  Torr. The deposition rates for Cu and Fe were determined by low-angle x-ray reflectivity measurements on single layer films and found to be 2.1 and 1.2 Å/s, respectively. The samples were

prepared at room temperature to minimize interdiffusion of Cu and Fe, and capped with 15 Å of Cu to reduce oxidation effects.

Sample structures were characterized by low- and high-angle x-ray diffraction (XRD) using Cu  $K$  radiation with the scattering vector perpendicular to the film surface. Magnetotransport measurements between 77 and 300 K were carried out using a high-resolution ac bridge. The ac susceptibility and magnetization of samples were measured between 5 and 290 K using a commercial ac susceptometer. Conversion-electron Mössbauer spectroscopy (CEMS) measurements were performed at room temperature using a gas-flow proportional counter with premixed He/4% CH<sub>4</sub>. CEMS data were analyzed using a nonlinear least-squares fitting with overlapped Lorentzian curves to obtain the hyperfine parameters. Typical linewidths (half width at half maximum) were  $\sim 0.25$  mm/s. All isomer shifts given below are relative to bulk  $\alpha$ -Fe at room temperature.

### III. STRUCTURAL CHARACTERIZATION

Two single 500 Å (nominal) films of Cu and Fe were prepared for thickness calibration purposes on silicon substrates. To estimate the actual layer thicknesses, the low-angle x-ray diffraction data were fitted using a standard optical model,<sup>16,17</sup> in which the x-ray reflectivity is calculated using a matrix method. Possible interfacial mixing has been incorporated into the calculation by assuming a linear composition profile. Also global roughness and layer thickness fluctuations were added to simulate a realistic system. Using a nonlinear least-squares fitting procedure, the layer thicknesses of Cu and Fe were deduced to be  $708 \pm 1$  Å and  $612 \pm 2$  Å, respectively, compared to the nominal 500 Å.

Cu/Fe multilayers with nominal bilayer period  $\Lambda$  ranging from 30 to 50 Å and bilayer numbers  $N$  of 12–36 were checked by x-ray reflectivity and analyzed using the same optical model. Figure 1 shows the x-ray reflectivity spectra for the series of multilayers with  $N=12$  and 36, and a fixed nominal Cu layer thickness  $t_{\text{Cu}}$  of 25 Å. Correcting the nominal layer thicknesses,  $t_{\text{Cu}}$  and  $t_{\text{Fe}}$ , based on the calibration data, the deduced layer thicknesses were found to be within 10% of the calibrated values. Bragg peaks up to the fourth order are visible in both figures without apparent peak broadening, indicating a well-defined compositional modulation along the film growth direction. However, the reduction in the Bragg peak intensities with decreasing  $t_{\text{Fe}}$  indicates the presence of interface roughness. In every sample analyzed, the fitted roughness of the Fe/Cu interface  $\sigma_{\text{Fe/Cu}}$  (Cu deposited on Fe) was larger than that of the Cu/Fe interface  $\sigma_{\text{Cu/Fe}}$  (Fe deposited on Cu) and was found to increase with  $t_{\text{Fe}}$ . The observed difference in the roughnesses  $\sigma_{\text{Fe/Cu}}$  and  $\sigma_{\text{Cu/Fe}}$  can be explained by interfacial disorder due to the lattice mismatch. In equilibrium, Cu exists only in a fcc structure, whereas Fe can exist in both bcc and fcc forms.<sup>18</sup> When an ultrathin Fe layer is grown on a stable fcc Cu layer, epitaxial growth may produce fcc Fe with a negligible lattice mismatch.<sup>6,19</sup> Thus Fe grows smoothly as fcc on the Cu, ( $\sigma_{\text{Cu/Fe}}$  small), and Cu again grows smoothly on the fcc Fe ( $\sigma_{\text{Fe/Cu}}$  also small). This is consistent with the observation that  $\sigma_{\text{Cu/Fe}}$  is smallest in multilayers with nominal  $t_{\text{Fe}} = 5$  Å. As  $t_{\text{Fe}}$  increases, Fe regains its stable bcc structure,

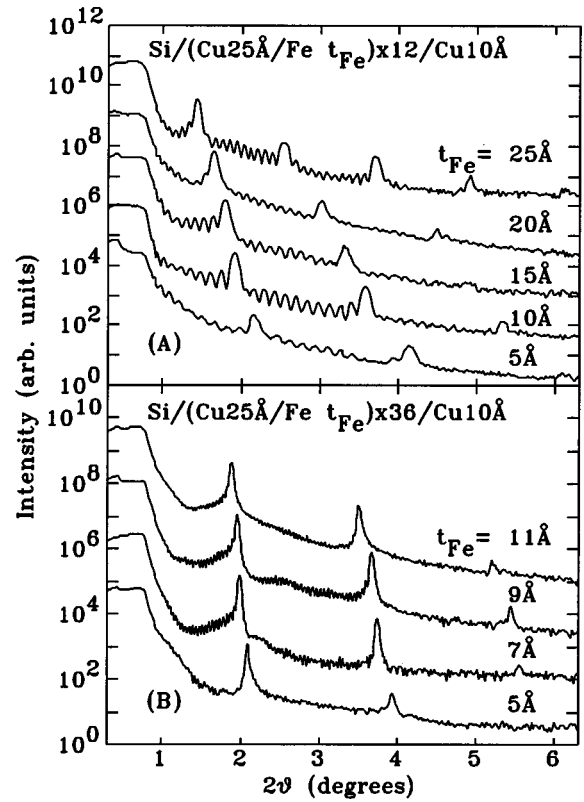


FIG. 1. Low-angle x-ray reflectivity data for (A) (Cu 25 Å/Fe  $t_{\text{Fe}}$ ) $\times$ 12 multilayers; and (B) (Cu 25 Å/Fe  $t_{\text{Fe}}$ ) $\times$ 36 multilayers. The spectra have been shifted vertically for clarity.

requiring a relatively large distortion to accommodate the subsequent growth of fcc Cu on the bcc Fe. Hence when Cu is grown on thicker Fe underlayers, larger values of  $\sigma_{\text{Fe/Cu}}$  may be expected. In the case of Fe deposited on Cu, the very first few layers will form fcc Fe with a smoother transition to bcc Fe ( $\sigma_{\text{Cu/Fe}} < \sigma_{\text{Fe/Cu}}$ ). Interfacial mixing can also cause significant roughness. Although the mutual solubility of Cu and Fe are negligible,<sup>7,20</sup> sputtering is a nonequilibrium process, and alloys with enhanced solid solubilities at the interfaces can be formed.<sup>5,21</sup> An island structure of dislocated submultilayers, due to structural disorder along the growth direction, also leads to large interface roughness.

Throughout this paper, the nominal layer thickness will be used to identify multilayer samples; however, for data presentation and analysis, the actual thickness has been used. To avoid ambiguity, whenever the nominal values are used, they will be identified explicitly. The nominal and actual layer thicknesses for all of the samples studied here are listed in Table I.

Every sample studied was checked by high-angle x-ray diffraction. For a series of (Cu 25 Å/Fe  $t_{\text{Fe}}$ ) $\times$ 36 multilayers, we observed two significant features: (1) the position of the main diffraction peak shifts to higher angles with increasing  $t_{\text{Fe}}$ ; and (2) the linewidths of the diffraction peaks increase monotonically with  $t_{\text{Fe}}$ . For the nominal  $t_{\text{Fe}} = 5$  Å multilayer, the main diffraction peak corresponds to Cu (111), but the peak is shifted slightly to higher angles. The small decrease in lattice spacing may indicate that a very small amount of Fe is dissolved in this structure as the Fe atom is about 1.5% smaller than the Cu atom. As the Bragg peaks for fcc (111) and bcc (110) for Fe occur at the same

TABLE I. Nominal and actual layer thicknesses of the  $(\text{Cu } t_{\text{Cu}}/\text{Fe } t_{\text{Fe}}) \times N$  multilayers used in this work.

$N$	Nominal	Actual
12	Cu 25 Å/Fe 25 Å	Cu 38.5 Å/Fe 34 Å
	Cu 25 Å/Fe 15 Å	Cu 38 Å/Fe 16.8 Å
	Cu 25 Å/Fe 10 Å	Cu 38 Å/Fe 11.5 Å
	Cu 25 Å/Fe 5 Å	Cu 38 Å/Fe 5.6 Å
36	Cu 25 Å/Fe 11 Å	Cu 39 Å/Fe 12.8 Å
	Cu 25 Å/Fe 9 Å	Cu 39 Å/Fe 10.4 Å
	Cu 25 Å/Fe 7 Å	Cu 38.5 Å/Fe 9.8 Å
	Cu 25 Å/Fe 5 Å	Cu 38.5 Å/Fe 7.3 Å

diffraction angle, it is difficult to distinguish the two structures. As  $t_{\text{Fe}}$  increases, the main diffraction peak becomes broader and shifts to higher diffraction angles. This implies that there is proportionally more Fe dissolved in fcc Cu due to interfacial mixing and/or that the amount of crystalline Fe (bcc or fcc) is increasing as  $t_{\text{Fe}}$  is increased.

#### IV. MAGNETOTRANSPORT PROPERTIES

The transversal magnetoresistance (transversal-MR) for all the samples was measured in magnetic fields of up to 0.1 T at temperatures between  $T=77$  and 295 K. Figure 2 shows the room-temperature transversal-MR for a series of  $(\text{Cu } 25 \text{ Å}/\text{Fe } t_{\text{Fe}}) \times 36$  multilayers with nominal  $t_{\text{Fe}}$  varying between 5 and 11 Å. The MR curve for nominal  $t_{\text{Fe}}=5$  Å is linear and shows no sign of saturation, indicating the absence of ferromagnetic Fe. The significant increase in transversal-MR for nominal  $t_{\text{Fe}}=7$  Å, indicates the presence of ferromagnetic  $\alpha$ -Fe in the multilayer. With increasing  $t_{\text{Fe}}$ , the magnitude of MR decreases due to additional bulk scat-

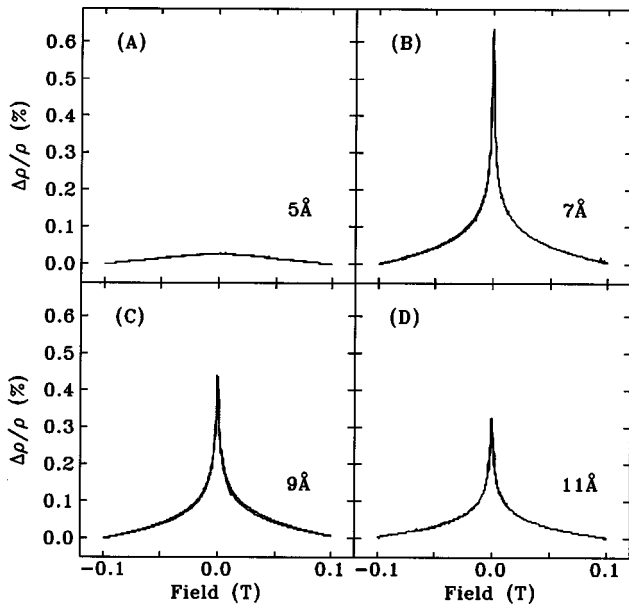


FIG. 2. Magnetoresistance measurements taken at room temperature for a series of  $(\text{Cu } 25 \text{ Å}/\text{Fe } t_{\text{Fe}}) \times 36$  with nominal  $t_{\text{Fe}}$  of (A) 5 Å; (B) 7 Å; (C) 9 Å; and (D) 11 Å. The magnetic field was applied in the plane of the multilayers perpendicular to the current direction (transversal-MR).

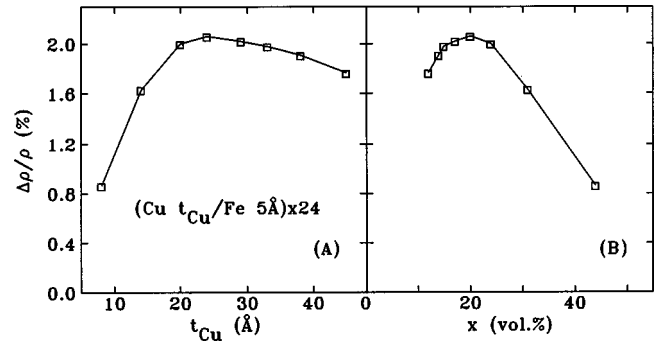


FIG. 3. Variation of MR as a function of: (A)  $t_{\text{Cu}}$  for  $(\text{Cu } t_{\text{Cu}}/\text{Fe } 5 \text{ Å}) \times 24$  multilayers; and (B) the equivalent Fe volume fraction  $x$  for  $(\text{Cu } t_{\text{Cu}}/\text{Fe } 5 \text{ Å}) \times 24$  multilayers. The measurements were taken at  $T=77$  K. The magnetic field of 0.1 T was applied in the plane of the multilayers perpendicular to the current direction. The values of  $t_{\text{Cu}}$  are calibrated thicknesses estimated from the x-ray reflectivity data. The solid lines are guides for the eye.

tering in Fe layers. The MR measurements with the field applied in the sample plane along the current direction (longitudinal-MR) were identical to the transversal-MR data. This isotropy is a characteristic of the giant magnetoresistance (GMR) effect.

The loss of GMR confirms that decreasing  $t_{\text{Fe}}$  leads to a change from ferromagnetism to paramagnetism. The magnetotransport measurements can help us to understand the structural properties of the multilayers by probing the interlayer exchange coupling. The variation of MR as a function of  $t_{\text{Cu}}$  for  $(\text{Cu } t_{\text{Cu}}/\text{Fe } 20 \text{ Å}) \times 24$  multilayers illustrated the oscillatory behavior of interlayer exchange coupling.<sup>22</sup> Peak positions and the overall profile of MR versus  $t_{\text{Cu}}$  were similar to those observed at 4.2 K in Fe/Cu multilayers with stable bcc Fe layers reported by Petroff *et al.*<sup>23</sup> This confirms that a Cu/Fe multilayer with nominal  $t_{\text{Cu}}=20$  Å has a well-defined superlattice structure with stable bcc Fe layers. Because the interlayer exchange coupling depends primarily on the Fermi surface and crystal structure of the spacer material,<sup>24,25</sup> well-defined Cu/Fe multilayers should exhibit a similar oscillating behavior of MR, independent of  $t_{\text{Fe}}$ .

The variation of transversal-MR as a function of  $t_{\text{Cu}}$  for  $(\text{Cu } t_{\text{Cu}}/\text{Fe } 5 \text{ Å}) \times 24$  multilayers at 77 K in a field of 0.1 T, is shown in Fig. 3(A). It is evident from the figure that oscillatory exchange coupling is absent. In fact, the plateau shape shown in Fig. 3(A) is commonly observed in Fe-Cu and Fe-Ag granular alloys.<sup>26–28</sup> This is more apparent in Fig. 3(B) where  $t_{\text{Cu}}$  is replaced by the equivalent volume fraction  $x$  of Fe. The maximum GMR was achieved with nominal  $t_{\text{Cu}}$  ranging from 20 to 30 Å, which corresponds to a moderate volume fraction range ( $15\% \leq x \leq 25\%$ ). The decrease in MR with increasing  $t_{\text{Cu}}$  (i.e., the Fe-poor region) results from a reduced magnetic scattering due to the low concentrations of Fe particles. At the other end, the weakening of MR with decreasing  $t_{\text{Cu}}$  (i.e., the Fe-rich region) can be explained by the loss of antiferromagnetic (AF) coupling between adjacent magnetic layers. The loss of AF coupling can be caused by structural imperfections such as pinholes in the nonmagnetic spacer layer. Such defects can give rise to strong direct ferromagnetic bridging of adjacent magnetic layers, leading to the loss of AF coupling and hence the decrease in MR.

The variation of MR with  $t_{\text{Cu}}$  indicates that for nominal

$t_{\text{Fe}}=20 \text{ \AA}$  the samples have a well-defined superlattice structure, whereas for nominal  $t_{\text{Fe}}=5 \text{ \AA}$  they are granular alloys due to island formation. These measurements illustrate a possible use of magnetotransport measurements as a structural characterization technique.

### V. MAGNETIC MEASUREMENTS

As superparamagnetism exhibits a characteristic temperature dependence,<sup>29,30</sup> ac susceptibility ( $\chi_{\text{ac}}$ ) enables us to distinguish the relative contribution of superparamagnetic phase from those of the nonmagnetic Cu-Fe alloy and fcc Fe phase. Figure 4(A) illustrates direct evidence of superparamagnetism and the associated blocking phenomenon observed in a (Cu 25 Å/Fe 5 Å)×12 multilayer. The easy magnetic axes of the single-domain grains in the multilayer are randomly oriented, and at sufficiently low temperatures, the magnetizations will be frozen in space. On warming, the susceptibility ( $\chi_{\text{ac}}$ ) grows as the thermal energy allows the grain magnetizations to fluctuate. At some temperature,  $T_B$  (often called the blocking temperature), the fluctuation rate matches the measurement frequency and  $\chi_{\text{ac}}$  reaches its maximum value. At higher temperatures  $\chi_{\text{ac}}$  falls as the fluctuations become too rapid to follow. Using an instrument with a characteristic measuring time  $\tau_i$ , the observed  $T_B$  for a sample with the characteristic time  $\tau_0$  is given as<sup>29</sup>

$$T_B = \frac{KV}{k_B[\ln(\tau_i/\tau_0)]}, \quad (1)$$

where  $KV$  is the barrier to magnetization reversal. Figure 4(A) shows that  $T_B$  at 377 Hz for a (Cu 25 Å/Fe 5 Å)×12 multilayer is  $\sim 205 \text{ K}$ . No blocking behavior was observed up to 300 K for a (Cu 25 Å/Fe 10 Å)×12 multilayer [Fig. 4(B)] indicating that either islands are absent, or that they are large enough that their blocking temperature lies above 300 K.

The temperature dependence of the initial susceptibility can also be used to determine the magnetic grain size in a superparamagnetic system. Taking the interaction effect between magnetic particles into consideration, Chantrel and Wohlfarth<sup>28,31</sup> found that the susceptibility  $\chi$ , of ultrafine particle systems with saturation magnetization  $M_s$ , density  $\rho$ , and volume  $V$  can be described by a Curie-Weiss-type law:

$$\chi = \frac{M_s^2(T)\rho V}{3k_B(T-T_0)} \quad \text{for } k_B T > \mu H, \quad (2)$$

where  $\mu (=M_s \rho V)$  is the magnetic moment of a single particle. The effective Curie temperature  $T_0$  indicates the strength of interaction and is marked by the intercept of  $1/\chi \rightarrow 0$  at the  $T$  axis. The temperature dependence of  $M_s(T)$  is due to spin-wave excitations inside the single-domain grains at finite temperatures. From Eq. (2), one can plot  $\sqrt{\chi(T-T_0)} = \sqrt{V/3k_B} M_s(T)$  as a function of  $T$  and extrapolate the curve to  $T \rightarrow 0 \text{ K}$  to obtain the intercept  $\sqrt{V/3k_B} M_s(0)$ . Then using the value of  $M_s$  measured at low  $T$ , we can calculate the average volume  $V$  of the grains from the intercept. Using the region  $T > T_B$  of the initial susceptibility measurement for a (Cu 25 Å/Fe 5 Å)×12 multilayer

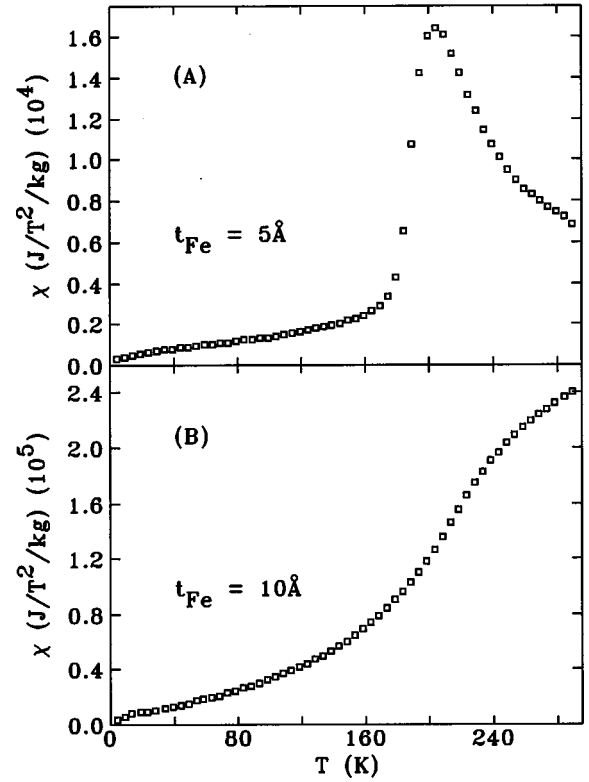


FIG. 4. Temperature dependence of zero-field-cooled magnetic susceptibility for (Cu 25 Å/Fe  $t_{\text{Fe}}$ )×12 multilayers with  $t_{\text{Fe}}=5 \text{ \AA}$  (A) and  $10 \text{ \AA}$  (B).

[shown in Fig. 4(A)], we estimate the diameter of spherical Fe grains to be  $2r_0 = 72 \pm 6 \text{ \AA}$ . However, a multilayer structure is likely to be isotropic within the growth plane, so it is more appropriate to consider the shape of the grains to be oblate ellipsoids with major axis  $a$  and minor axis  $c$ . With  $2c$  set equal to the Fe layer thickness  $t_{\text{Fe}}$ ,  $2a$  is estimated to be  $260 \pm 38 \text{ \AA}$ .

dc magnetization measurements were performed, along with the  $\chi_{\text{ac}}$  measurements, over a temperature range of 250 down to 5 K. Figure 5(A) shows, after subtracting the substrate contribution, the magnetization curve for

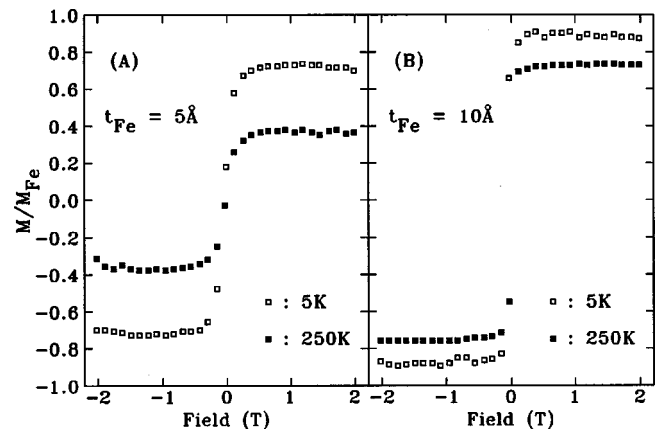


FIG. 5. Magnetization measurements taken at 5 K (empty squares) and 250 K (full squares) for (Cu 25 Å/Fe  $t_{\text{Fe}}$ )×12 multilayers with  $t_{\text{Fe}}=5 \text{ \AA}$  (A) and  $10 \text{ \AA}$  (B).

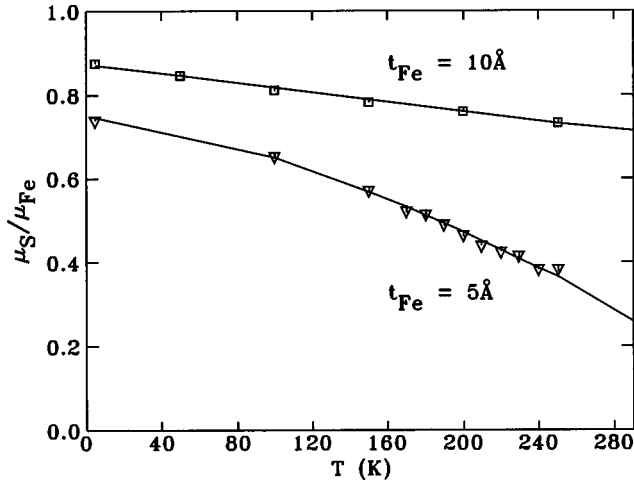


FIG. 6. Temperature dependence of the saturated Fe magnetic moment for (Cu 25 Å/Fe  $t_{\text{Fe}}$ ) $\times$ 12 multilayers with  $t_{\text{Fe}}=5$  Å (triangles) and 10 Å (squares).

(Cu 25 Å/Fe 5 Å) $\times$ 12 at temperatures of 5 K (empty squares) and 250 K (full squares). The magnetic moments of the sample were normalized by the expected moment of bulk  $\alpha$ -Fe. One should note that there exists a systematic scale uncertainty of  $\sim 12\%$  originating primarily from the uncertainty in  $t_{\text{Fe}}$ . It is interesting to observe a saturated moment even at 250 K, well above the observed  $T_B$  of  $\sim 205$  K, where paramagnetic behavior might be expected. The origin of this difference lies in the fields used in the measurements. The saturation in Fig. 5(A) was achieved with an applied field larger than 0.5 T, whereas  $\chi_{\text{ac}}$  was measured in 0.5 mT. The magnetization measurements for (Cu 25 Å/Fe 10 Å) $\times$ 12 are shown in Fig. 5(B). Smaller saturation fields and the large saturated moment, slightly less than that of bulk Fe, confirm the presence of the ferromagnetic  $\alpha$ -Fe phase.

The temperature dependence of the saturated Fe magnetic moment for (Cu 25 Å/Fe  $t_{\text{Fe}}$ ) $\times$ 12 multilayers with nominal  $t_{\text{Fe}}$  of 5 Å (triangles) and 10 Å (squares) is shown in Fig. 6. The sample with nominal  $t_{\text{Fe}}=10$  Å exhibits a linear dependence of magnetization with temperature:

$$\mu_s(T) = \mu_0(1 - bT), \quad (3)$$

which may be associated with a two-dimensional magnetic system.<sup>27</sup> The intercept  $\mu_0$  is the ground-state atomic magnetic moment of Fe. For a superparamagnetic system, it has been shown experimentally that  $\sqrt{\chi(T-T_0)}$  has a  $T^{3/2}$  dependence,<sup>29,32</sup> and hence  $\mu_s$  obeys Bloch's law:

$$\mu_s(T) = \mu_0(1 - BT^{3/2}), \quad (4)$$

where  $B$  is the spin-wave constant. From the fitting of the calculations to the experimental data (solid lines in Fig. 6),  $\mu_0$  were found to be 75 and 88 % of the value of the bulk Fe metal ( $\mu_{\text{Fe}}=2.21\mu_B$ ) for nominal  $t_{\text{Fe}}=5$  and 10 Å, respectively. Assuming that the average Fe moment in the multilayers is identical to that of bulk Fe, the results indicate that for nominal  $t_{\text{Fe}}=5$  Å most of the Fe atoms (75%) are in the superparamagnetic Fe phase. The remaining 25 and 12 % of the Fe atoms in the samples with nominal  $t_{\text{Fe}}=5$  and 10 Å, respectively, are present as nonmagnetic phases, such as an interfacial Cu-Fe alloy. Although it has been reported that

fcc-Fe orders with a Néel temperature of about 67 K (Refs. 33,34) neither the  $\chi_{\text{ac}}$  measurements nor the temperature dependence of the magnetization showed any evidence for such an ordering.

## VI. CONVERSION ELECTRON MÖSSBAUER SPECTROSCOPY

It is clear from the magnetic properties of the multilayers, that Fe atoms exist in a variety of environments depending on the value of  $t_{\text{Fe}}$ . It is essential, therefore, to utilize a local probe which will provide information that is complementary to that obtained from x-ray diffraction. Figure 7 shows CEMS data for a series of (Cu 25 Å/Fe  $t_{\text{Fe}}$ ) $\times$ 36 multilayers with nominal  $t_{\text{Fe}}$  ranging from 11 down to 5 Å. The first two Mössbauer spectra (nominal  $t_{\text{Fe}}=9$  and 11 Å) were found to be a superposition of two sextets (sextet A and sextet B), and one doublet (doublet A). Both sextets come from Fe atoms in a bulklike ferromagnetic bcc phase consistent with the transversal-MR results. Sextet A is due to atoms with only Fe nearest neighbors while sextet B, with a smaller  $B_{\text{HF}}$  is attributed to Fe with some Cu neighbors, presumably at the Fe-Cu interfaces.<sup>5</sup> The doublet originates from the electric quadrupole interaction in a nonmagnetic phase, and we attribute it to a distorted interfacial Fe-Cu alloy. An additional nonmagnetic component, (doublet B) appears in the spectrum of the nominal  $t_{\text{Fe}}=7$  Å sample. This component has a smaller quadrupole splitting than doublet A, and an isomer shift closer to zero. Finally, the nominal  $t_{\text{Fe}}=5$  Å, the CEMS spectrum shows no magnetic contribution, and consists only of doublets A and B. For the three thinnest samples (nominal  $t_{\text{Fe}}=9, 7,$  and 5 Å) the doublets exhibit a clear asymmetry in intensity ( $R$  in Table II) reflecting highly textured growth. Similar line asymmetries have been reported in epitaxial Fe/Cu(001) films<sup>13</sup> but with the sense reversed. The relevant parameters extracted from least-squares fitting of the spectra are summarized in Table II.

A visual examination of the CEMS data in Fig. 7 shows that decreasing  $t_{\text{Fe}}$  leads to a transition from ferromagnetism to paramagnetism and that both the average hyperfine field (Fig. 8)  $B_{\text{HF}}$  and the volume fraction  $V_F$  of the ferromagnetic phases decrease monotonically with  $t_{\text{Fe}}$ . The dotted horizontal line in Fig. 8(A) represents the hyperfine field of bulk  $\alpha$ -Fe, (33 T). For sufficiently thick  $t_{\text{Fe}}$  ( $t_{\text{Fe}}\geq 34$  Å), Fe in a Cu/Fe multilayer has bulklike  $\alpha$ -Fe properties, with  $R=4$  indicating in-plane magnetization. The decline in  $\langle B_{\text{HF}} \rangle$  reflects both an increasing proportion of the interfacial Fe(Cu) alloy, and also the onset of superparamagnetic fluctuations as the layers start to break up into islands with decreasing  $t_{\text{Fe}}$ . A gradual magnetic evolution occurs with decreasing  $t_{\text{Fe}}$  until the magnetic contribution disappears for ultrathin  $t_{\text{Fe}}$  ( $\leq 7$  Å).

Analysis of the various components seen in the CEMS data can be used to shed some light on the structural changes that occur as  $t_{\text{Fe}}$  is reduced. Working from a Cu base layer, through an Fe layer and back to Cu, we make the following assignments.

The assignment of doublet A is the most problematic. Its steady growth in area as the Fe layer thickness is reduced, indicates that it involves a constant  $\sim 1.7$  Å of the iron in

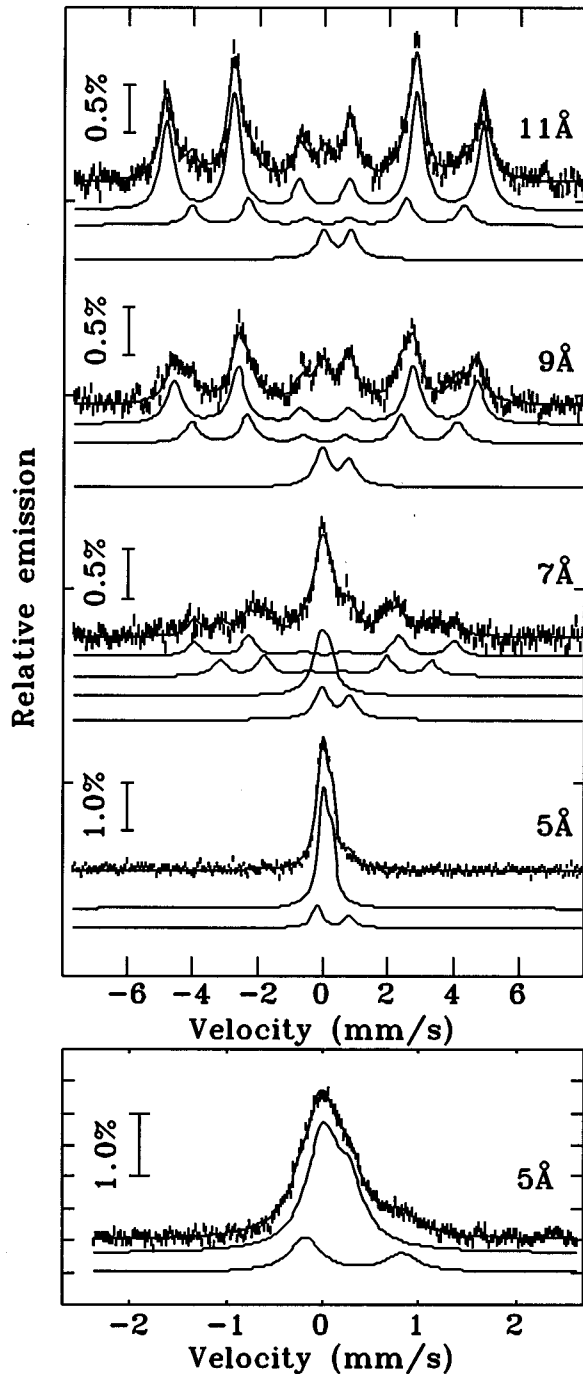


FIG. 7. Conversion-electron Mössbauer spectra taken at room temperature (vertical bars) and the calculated fits (solid lines) for a series of  $(\text{Cu } 25 \text{ \AA}/\text{Fe } t_{\text{Fe}}) \times 36$  with nominal  $t_{\text{Fe}}$  ranging from 11 down to 5 Å. The relevant parameters extracted from least-squares fitting of the spectra are listed in Table II.

each layer [Fig. 9(A)], and that it is therefore probably associated with an interfacial Fe-Cu alloy. However, while the hyperfine parameters are stable across the series of samples ( $\delta \sim 0.35 \text{ mm/s}$ ,  $\Delta \sim 0.85 \text{ mm/s}$ ) they are somewhat larger than those found in dilute Cu(Fe) alloys [ $\delta = 0.225 \text{ mm/s}$  (Ref. 35),  $\Delta = 0.45 \text{ mm/s}$  (Ref. 21)]. Larger quadrupole splittings have been reported for Fe clusters in Cu  $\Delta = 0.60 \text{ mm/s}$  (Ref. 36) and epitaxial Fe grown on Cu(001)  $\Delta = 0.62 \text{ mm/s}$ ,<sup>13</sup> however, the isomer shifts in each case are

close to zero. An alternative assignment for this component is a ferric oxide (ferrous oxides would not be consistent with either observed Mössbauer parameter). Such an oxide would be consistent with the observed isomer shift, and cannot be ruled out, however it is inconsistent with several other observations: (i) the ferric oxides (haematite, maghemite, and magnetite) all have magnetic ordering temperatures well above RT so we might expect such an impurity to yield a magnetically split spectrum. (ii) Very small magnetic oxide particles would be superparamagnetic and could give a non-magnetic contribution at RT, but low-temperature Mössbauer measurements on these samples show no ordering of this component down to 90 K.<sup>37</sup> Furthermore, our susceptibility data Fig. 4(A), also shows no evidence of additional ordering of an impurity phase down to 5 K. (iii) The constant thickness ( $\sim 1.7 \text{ \AA}/\text{layer}$ ) of this phase is more consistent with an interfacial alloy than an oxide formed during production or subsequent storage. (iv) There was no change in the amount of this phase present after storage for 18 months in ambient air. We, therefore, prefer to identify this component as an interfacial Fe-Cu alloy, and attribute the large  $\delta$  and  $\Delta$  values to strains associated with the multilayer structure.

Sextet A is simply bulklike bcc-Fe formed in the centers of the Fe layers, while sextet B is an Fe(Cu) alloy and originates from the Fe/Cu interfaces (Cu grown on Fe). The slightly reduced  $B_{\text{HF}}$  reflects the presence of some Cu neighbors. Thus different Fe phases form at the Cu/Fe and Fe/Cu interfaces, an interpretation that is consistent with the different roughnesses of the two interfaces, and also with similar distinctions reported for Fe/Sb and Sb/Fe interfaces.<sup>38</sup> Furthermore, it is clear from Fig. 9(A) that the nonmagnetic Cu-Fe layer at the Cu/Fe interface is significantly thinner than the magnetic bcc-Fe(Cu) layer at the Fe/Cu interface, a result that is fully consistent with the low-angle XRD observation of  $\sigma_{\text{Cu/Fe}} < \sigma_{\text{Fe/Cu}}$ .

Doublet B is only observed in the two thinnest samples (nominal  $t_{\text{Fe}} = 7$  and 5 Å) and its appearance is correlated with the loss of the magnetic components. It exhibits the same strong intensity asymmetry as the other paramagnetic doublet, again reflecting textured growth. Low-temperature CEMS data<sup>37</sup> shows that this phase orders around 200 K and is the origin of the peak in the susceptibility in Fig. 4(A). We attribute this component to Fe in a distorted fcc structure, i.e., fct-Fe. This phase exhibits perpendicular anisotropy below  $T_c \sim 200 \text{ K}$  (Ref. 37) consistent with surface magneto-optic Kerr effect (SMOKE) data on epitaxial wedges.<sup>11</sup> The fitted values for  $\Delta$  are somewhat larger than reported on Fe/Cu(001) epitaxial samples<sup>13</sup> but this may be due to additional strains associated with the iron being sandwiched between successive fcc-Cu layers, or related to our growth being on the Cu(111) surface. Reported ordering temperatures for thin-film fct-Fe range from  $>500 \text{ K}$ ,<sup>13</sup>  $370 \text{ K} > T_c > 280 \text{ K}$  (Ref. 9) to 250 K,<sup>11</sup> all well above our value of  $\sim 200 \text{ K}$ , which therefore reflects blocking of superparamagnetic islands rather than the ordering of fct-Fe. Indeed, since fct-Fe exhibits a substantial  $B_{\text{HF}}$ ,<sup>13</sup> it is likely that significant amounts of fct-Fe could be contributing to the two sextets, and it only becomes apparent as a distinct phase when the islands become small enough to be superparamagnetic at RT.

Based on this structural interpretation of the CEMS data, the following picture emerges as an explanation for the ob-

TABLE II. Hyperfine parameters extracted from fitting the spectra shown in Fig. 7 for a series of (Cu 25 Å/Fe  $t_{\text{Fe}}$ ) $\times$ 36 multilayers with nominal  $t_{\text{Fe}}$  ranging from 11 down to 5 Å. Here,  $\delta$  is the isomer shift;  $\Delta$  is the quadrupole splitting; for the magnetic subspectra,  $R$  is the intensity ratio of lines 2 and 5 to those of line 3 and 4, while for the doublets,  $R$  is the intensity ratio of the low and high velocity lines,  $B_{\text{HF}}$  is the hyperfine field; and  $V$  is the fractional area of each subspectrum.

(Cu/Fe) $\times$ $N$	Subspectra	$\delta$ (mm/s)	$\Delta$ (mm/s)	$R$	$B_{\text{HF}}$ (T)	$V$ (%)
(25 Å/11 Å) $\times$ 36	Sextet A	0.01 $\pm$ 0.01		4.00 $\pm$ 0.12	30.2 $\pm$ 0.1	74 $\pm$ 2
	Sextet B	0.10 $\pm$ 0.02		4.00 $\pm$ 0.12	25.9 $\pm$ 0.2	17 $\pm$ 2
	Doublet A	0.40 $\pm$ 0.03	0.86 $\pm$ 0.05	1.00 $\pm$ 0.19		9 $\pm$ 2
(25 Å/9 Å) $\times$ 36	Sextet A	0.04 $\pm$ 0.01		4.00 $\pm$ 0.17	28.9 $\pm$ 0.1	56 $\pm$ 2
	Sextet B	0.01 $\pm$ 0.02		4.00 $\pm$ 0.17	25.3 $\pm$ 0.2	28 $\pm$ 2
	Doublet A	0.36 $\pm$ 0.03	0.85 $\pm$ 0.04	1.45 $\pm$ 0.21		16 $\pm$ 2
(25 Å/7 Å) $\times$ 36	Sextet A	0.02 $\pm$ 0.03		4.00 $\pm$ 0.40	24.8 $\pm$ 0.2	28 $\pm$ 2
	Sextet B	0.07 $\pm$ 0.03		4.00 $\pm$ 0.40	20.2 $\pm$ 0.2	27 $\pm$ 2
	Doublet A	0.39 $\pm$ 0.06	0.88 $\pm$ 0.11	1.40 $\pm$ 0.45		18 $\pm$ 2
	Doublet B	0.03 $\pm$ 0.04	0.27 $\pm$ 0.07	1.40 $\pm$ 0.45		27 $\pm$ 2
(25 Å/5 Å) $\times$ 36	Doublet A	0.326 $\pm$ 0.012	0.999 $\pm$ 0.022	1.85 $\pm$ 0.13		23 $\pm$ 2
	Doublet B	0.132 $\pm$ 0.006	0.266 $\pm$ 0.007	1.85 $\pm$ 0.13		77 $\pm$ 2

served magnetic changes. With decreasing  $t_{\text{Fe}}$ , the bulklike bcc  $\alpha$ -Fe layer gets thinner, and hence the relative contribution of the ferromagnetic sextets falls. The pure-Fe regions undergo a transformation from bcc to fct around  $t_{\text{Fe}}=10$  Å, but this phase is also ordered above RT and so cannot cause

the loss of ferromagnetic order. Some of the loss of magnetic order comes from the growing importance of the  $\sim 1.7$  Å layer of Cu-Fe alloy, however, the biggest change in magnetic properties is associated with the breakup of the layers into isolated superparamagnetic fct-Fe islands. The bcc-fct transformation must occur before the islands become super-

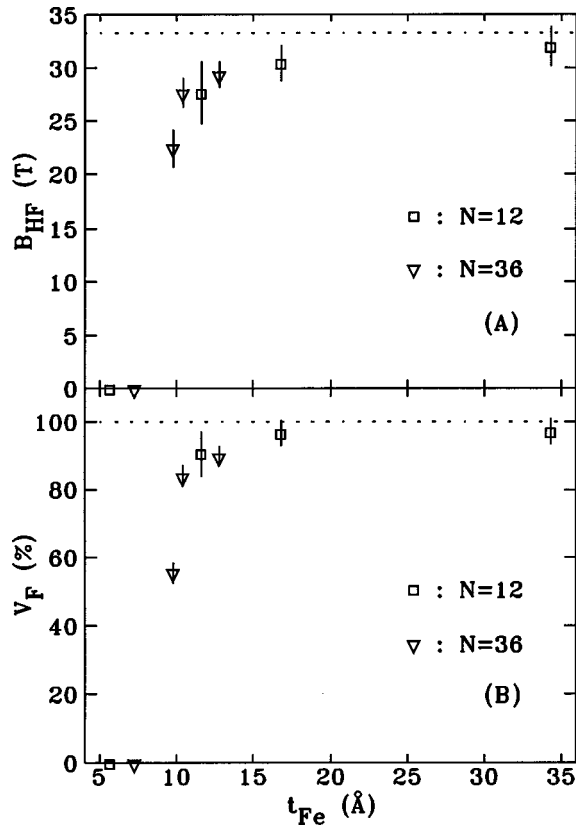


FIG. 8.  $t_{\text{Fe}}$  dependence of (A) the average hyperfine field  $B_{\text{HF}}$  and (B) the fractional volume  $V_F$  of the ferromagnetic phases. The values were extracted from least-squares fitting of CEMS spectra for (Cu 25 Å/Fe  $t_{\text{Fe}}$ ) $\times$  $N$  multilayers with  $N=12$  (squares) and 36 (triangles). The dotted line in (A) represents the hyperfine field of bulk  $\alpha$ -Fe, 33 T.

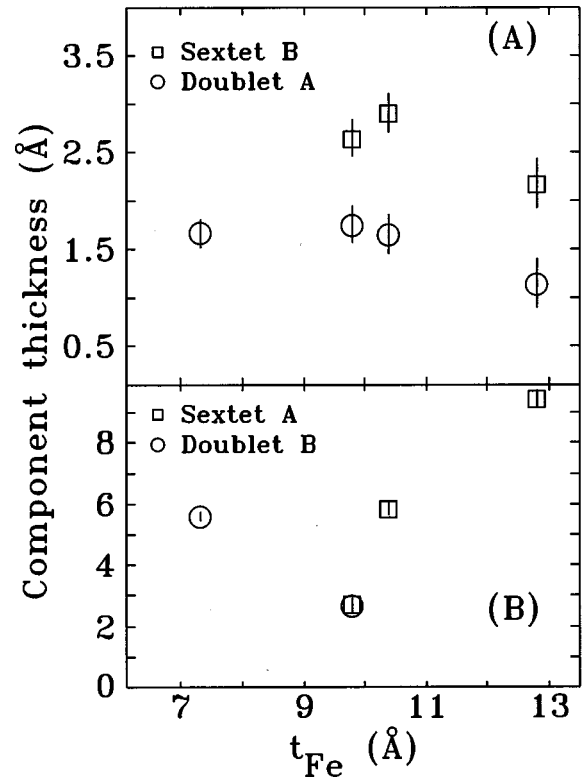


FIG. 9.  $t_{\text{Fe}}$  dependence of the thicknesses of the four identified components in the CEMS data. (A) the two interfacial phases: Cu-Fe alloy (doublet A) and the bcc-Fe (Cu) alloy (sextet B). Note that in both cases the interfacial alloys have essentially constant thicknesses. (B) The two primary components: bcc-Fe (sextet A) and fct-Fe (doublet B) showing the structural change at  $t_{\text{Fe}} \sim 10$  Å.

paramagnetic as we never observe a contribution from superparamagnetic bcc-Fe (a singlet centred at zero velocity). The thinnest sample shows only paramagnetic components at RT interfacial Cu-Fe alloy (doublet *A*) and superparamagnetic fct-Fe (doublet *B*). The CEMS results are fully consistent with the magnetic measurements and show the same trends. Magnetization at 5 K showed 25 and 12 % of the Fe atoms to be in nonmagnetic structures for nominal  $t_{\text{Fe}}=5$  and 10 Å, respectively, consistent with the area of the nonmagnetic component (fct-Fe is ferromagnetic at 5 K) in the CEMS spectra (23 and 16 % in the nominal  $t_{\text{Fe}}=5$  and 9 Å samples in Table II).

## VII. OVERALL DISCUSSION

Throughout this paper, we reported the observed evolution from ferromagnetism to paramagnetism at room temperature with decreasing  $t_{\text{Fe}}$  and tried to understand the structural changes responsible for the observed transition. Here we present a simple structural model that is consistent with our experimental results.

For sufficiently large  $t_{\text{Fe}}$ , the multilayer sample has a well-defined superlattice structure. This was verified by the observation of higher-order superlattice peaks in the low-angle x-ray reflectivity data and by the presence of the oscillatory exchange coupling in the magnetotransport measurements. The conversion-electron Mössbauer spectra (CEMS) suggested that the Fe layer can be divided into three sublayers, each with its own unique magnetic properties: (1) bulk-like ferromagnetic bcc Fe layer; (2) Fe-rich ferromagnetic Fe/Cu interfacial layer (Cu grown on Fe); (3) paramagnetic Cu-Fe alloy phase at the Cu/Fe interface. The contributions of the first two sublayers can be estimated from the fractional areas of sextets *A* and *B*, respectively, in the CEMS spectra, while the contribution of the third sublayer is related to the fractional area of doublet *A*. Decreasing  $t_{\text{Fe}}$  leads to a steady increase in the proportions of the two alloyed sublayers at the expense of the bcc-Fe layer, however, their estimated thicknesses remain constant. Below a certain critical thickness, a distorted fcc, i.e., fct structure becomes favorable,<sup>11</sup> and starts to replace the bcc-Fe, however the fct-Fe is still magnetic.

For sufficiently small  $t_{\text{Fe}} \leq 7$  Å, surface roughness leads to structural imperfections and causes island formation, resulting in a granular-solid structure. Doublet *B* appears in the CEMS spectra and the room-temperature magnetization falls rapidly. The magnetic transformation was confirmed by the magnetotransport and  $\chi_{\text{ac}}$  measurements. At this point, the Fe grains embedded in a Cu matrix can also be divided into two sublayers according to their magnetic properties: (1) a ferromagnetic fct Fe core; (2) an outermost paramagnetic Cu-Fe alloy phase. Below a critical size the Fe grains can accommodate only a single magnetic domain even in zero magnetic field. For sufficiently large  $t_{\text{Fe}} > t_c$ , the grains will be large and their blocking temperature  $T_B$  will lie above room temperature. However, on decreasing  $t_{\text{Fe}}$ , Fe grains will reach a size where  $T_B$  is below room temperature, leading to the apparent loss of ferromagnetism as superparamagnetic fluctuations dominate. In summary, the observed mag-

netic transition is likely due to superparamagnetic relaxation of fct-Fe islands rather than a structural transition from bcc Fe to paramagnetic fcc or fct Fe as  $t_{\text{Fe}}$  decreases below  $t_c$ .

## VIII. CONCLUSIONS

We have studied in detail the structural, magnetic, and magnetotransport properties of sputter-deposited Cu/Fe multilayers. Structural characterization by low-angle x-ray reflectivity confirmed the successful growth of a well-defined multilayer structure. The reduction of the higher-order superlattice Bragg peaks with decreasing  $t_{\text{Fe}}$  indicates the relatively increasing contribution of the interface roughness. High-angle x-ray diffraction showed that with increasing  $t_{\text{Fe}}$  the position of the main peak shifts from Cu(111) peak position to higher angles and the linewidth of the diffraction peaks increases. This can be explained by Fe atoms dissolved in fcc Cu medium due to interfacial mixing.

The loss of GMR effect for nominal  $t_{\text{Fe}}=5$  Å confirmed the change in magnetic behavior with decreasing  $t_{\text{Fe}}$ . The variation of MR with  $t_{\text{Cu}}$  indicated that for nominal  $t_{\text{Fe}}=20$  Å a multilayer has a well-defined superlattice structure, whereas a multilayer with nominal  $t_{\text{Fe}}=5$  Å has a granular-alloy-like structure. These magnetotransport measurements confirmed that a multilayer with nominal  $t_{\text{Fe}}=5$  Å has an island structure leading to superparamagnetic relaxation at room temperature.

$\chi_{\text{ac}}$  with a characteristic time  $\tau_{\text{ac}}$  of  $2.65 \times 10^{-3}$  s showed blocking behavior for nominal  $t_{\text{Fe}}=5$  Å with  $T_{B,\text{ac}}$  of around 205 K, providing direct evidence for the existence of a superparamagnetic phase. A simple calculation shows the diameter of spherical Fe grains to be  $260 \pm 38$  Å. dc magnetization measurements, performed along with the  $\chi_{\text{ac}}$  measurements, on nominal  $t_{\text{Fe}}=5$  Å sample showed a saturated magnetization corresponding to 39% of that of bulk  $\alpha$ -Fe at 250 K with an applied field larger than 0.5 T. The temperature dependence of the magnetization showed that the extrapolated 0 K magnetization of the multilayers could be accounted for by 75% and 88% of the bulk  $\alpha$ -Fe magnetization for nominal  $t_{\text{Fe}}=5$  and 10 Å, respectively. Assuming that the average Fe moment in the multilayers is identical to that of  $\alpha$ -Fe, 25% and 12% of the Fe atoms in the samples with nominal  $t_{\text{Fe}}=5$  and 10 Å, respectively, are present as a nonmagnetic Cu-Fe alloy.

The Mössbauer study confirmed the gradual evolution from ferromagnetism to paramagnetism with decreasing  $t_{\text{Fe}}$ . Doublet *A*, which gave an almost constant thickness contribution in all of the multilayers, was assigned to a Cu-Fe alloy phase at the Cu/Fe interfaces (Fe grown on Cu). The two magnetic components in the spectra were attributed to bulk-Fe and an Fe(Cu) alloy. These decreased in average hyperfine field and total area as the Fe layer thickness was reduced. An additional doublet appeared for nominal  $t_{\text{Fe}}=7$  and 5 Å and was attributed to superparamagnetic islands of fct-Fe. Since we saw no evidence of superparamagnetic bcc-Fe, and fct-Fe is ferromagnetic, we concluded that the bcc-fct transformation occurs before the islands become too small to be blocked at room temperature.

All of the magnetic and magnetotransport measurements suggest that with decreasing  $t_{\text{Fe}}$  the ultrathin Fe layers first transform into fct-Fe and then break up into small islands. It



is the latter process that results in the magnetic transition from ferromagnetism to superparamagnetism.

### ACKNOWLEDGMENTS

This research was supported by grants from the Natural Sciences and Engineering Research Council of Canada and

Fonds pour la Formation de Chercheurs et aide à la Recherche. We would also like to thank M. Cai, T. Veres, and R. W. Cochrane for valuable assistance with the magneto-transport measurements, and R. Abdouche and M. Sutton for their help with the low-angle x-ray reflectivity measurements.

- 
- <sup>1</sup>C. S. Wang, B. M. Klein, and H. Krakauer, *Phys. Rev. Lett.* **54**, 1852 (1985).
- <sup>2</sup>F. J. Pinski, J. Staunton, B. L. Gyorffy, D. D. Johnson, and G. M. Stocks, *Phys. Rev. Lett.* **56**, 2096 (1986).
- <sup>3</sup>V. L. Moruzzi, P. M. Marcus, K. Schwarz, and P. Mohn, *Phys. Rev. B* **34**, 1784 (1986).
- <sup>4</sup>W. A. Jesser and J. W. Matthews, *Philos. Mag.* **15**, 1097 (1967).
- <sup>5</sup>H. M. van Noort, F. J. A. den Broeder, and H. J. G. Draaisma, *J. Magn. Magn. Mater.* **51**, 273 (1985).
- <sup>6</sup>A. Clarke, P. J. Rous, M. Arnott, G. Jennings, and R. F. Willis, *Surf. Sci.* **192**, L843 (1987).
- <sup>7</sup>D. Pescia, M. Stampanoni, G. L. Bona, A. Vaterlaus, R. F. Willis, and F. Meier, *Phys. Rev. Lett.* **58**, 2126 (1987).
- <sup>8</sup>W. A. A. Macedo and W. Keune, *Phys. Rev. Lett.* **61**, 475 (1988).
- <sup>9</sup>J. Thomassen, F. May, B. Feldmann, M. Wittig, and H. Ibach, *Phys. Rev. Lett.* **69**, 3831 (1992).
- <sup>10</sup>S. F. Cheng, A. N. Mansour, J. P. Teter, K. B. Hathaway, and L. T. Kabacoff, *Phys. Rev. B* **47**, 206 (1993).
- <sup>11</sup>Dongqi Li, M. Freitag, J. Pearson, Z. Q. Qui, and S. D. Bader, *Phys. Rev. Lett.* **72**, 3112 (1994).
- <sup>12</sup>S. Müller, P. Bayer, C. Reischl, K. Heinz, B. Feldmann, H. Zillgen, and M. Wuttig, *Phys. Rev. Lett.* **74**, 765 (1995).
- <sup>13</sup>W. Keune, A. Schatz, R. D. Ellerbrock, A. Fuest, Katrin Wilmers, and R. A. Brand, *J. Appl. Phys.* **79**, 4265 (1996).
- <sup>14</sup>M. Komuro, Y. Kozono, S. Narishige, M. Hanazono, and Y. Sugita, *IEEE Trans. Magn.* **MAG-23**, 3701 (1987).
- <sup>15</sup>Q. A. Pankhurst, M. F. Thomas, C. E. Johnson, R. Zquiak, X. X. Zhang, and J. Tejada, *IEEE Trans. Magn.* **30**, 778 (1994).
- <sup>16</sup>Y. Huai, R. W. Cochrane, and M. Sutton, *Phys. Rev. B* **48**, 2568 (1993).
- <sup>17</sup>M. Born and E. Wolf, *Principles of Optics* (Pergamon, Oxford, 1964).
- <sup>18</sup>*Binary Alloy Phase Diagram*, edited by Thaddeus B. Massalski (American Society for Metals, Metals Park, OH, 1986).
- <sup>19</sup>P. Ehrhard, B. Schonfeld, H. H. Ettwig, and W. Pepperhoff, *J. Magn. Magn. Mater.* **22**, 79 (1980).
- <sup>20</sup>Rodney P. Elliott, *Constitution of Binary Alloys, First Supplement* (McGraw-Hill, New York, 1965).
- <sup>21</sup>M. M. Pereira de Azevedo, M. S. Rogalski, and J. B. Sousa, *Solid State Commun.* **100**, 639 (1996).
- <sup>22</sup>D. W. Lee, M.Sc. thesis, McGill University, 1997.
- <sup>23</sup>F. Petroff, A. Barthélemy, D. H. Mosca, D. K. Lottis, A. Fert, P. A. Schroeder, W. P. Pratt, Jr., R. Loloee, and S. Lequien, *Phys. Rev. B* **44**, 5355 (1991).
- <sup>24</sup>P. Bruno and C. Chappert, *Phys. Rev. B* **46**, 261 (1992).
- <sup>25</sup>P. Bruno and C. Chappert, *Phys. Rev. Lett.* **67**, 1602 (1991).
- <sup>26</sup>Gang Xiao, Jian Qing Wang, and Peng Xiang, *Appl. Phys. Lett.* **62**, 420 (1993).
- <sup>27</sup>Chubing Peng and Daosheng Dai, *J. Appl. Phys.* **76**, 2986 (1994).
- <sup>28</sup>Jian-Qing Wang and Gang Xiao, *Phys. Rev. B* **49**, 3982 (1994).
- <sup>29</sup>C. L. Chien, *J. Appl. Phys.* **69**, 5267 (1991).
- <sup>30</sup>C. P. Bean and J. D. Livingston, *J. Appl. Phys.* **30**, 120 (1959).
- <sup>31</sup>R. W. Chantrel and E. P. Wohlfarth, *J. Magn. Magn. Mater.* **40**, 1 (1983).
- <sup>32</sup>Gang Xiao and C. L. Chien, *J. Appl. Phys.* **61**, 3308 (1987).
- <sup>33</sup>U. Gonser, C. J. Meechan, A. H. Muir, and H. Wiedersich, *J. Appl. Phys.* **34**, 2373 (1963).
- <sup>34</sup>G. J. Johanson, M. B. McGirr, and D. A. Wheeler, *Phys. Rev. B* **1**, 3208 (1970).
- <sup>35</sup>R. Ingalls, F. Van Der Woude, and G. A. Sawatzky, in *Mössbauer Isomer Shifts*, edited by G. K. Shenoy and F. E. Wagner (North-Holland, New York, 1978), p. 409.
- <sup>36</sup>S. J. Campbell, P. E. Clark, and P. R. Liddell, *J. Phys. F* **2**, L114 (1972).
- <sup>37</sup>A. Kuprin, D. W. Lee, Z. Altounian, and D. H. Ryan, *J. Appl. Phys.* (to be published).
- <sup>38</sup>T. Shinjo, in *Metallic Superlattices*, edited by T. Shinjo and T. Takada (Elsevier, New York, 1987), p. 107.